ORIGINAL ARTICLE

Interaction Between Cerebellum and Cerebral Cortex, Evidence from Dynamic Causal Modeling

Qasim Bukhari[1] · Sebastian F. Ruf[2,3] · Xavier Guell[1,4] · Susan Whitfield-Gabrieli[1,2] · Sheeba Anteraper[2,5,6]

Abstract

The interaction of the cerebellum with cerebral cortical dynamics is still poorly understood. In this paper, dynamical causal modeling is used to examine the interaction between cerebellum and cerebral cortex as indexed by MRI resting-state functional connectivity in three large-scale networks on healthy young adults (N = 200; Human Connectome Project dataset). These networks correspond roughly to default mode, task positive, and motor as determined by prior cerebellar functional gradient analyses. We find uniform interactions within all considered networks from cerebellum to cerebral cortex, providing support for the notion of a universal cerebellar transform. Our results provide a foundation for future analyses to quantify and further investigate whether this is a property that is unique to the interactions from cerebellum to cerebral cortex.

Keywords Dynamic causal modeling · Cerebellum · Resting-state fMRI

Introduction

The cerebellum has been identified as an important contributor not only to motor functions but also to non-motor functions including cognition and affect [1]. Anatomical connections link the cerebellum to motor as well as non-motor territories of the cerebral hemispheres [2]. Clinical studies have shown that isolated cerebellar injury or degeneration is sufficient to produce motor, cognitive, and affective deficits [3–6], and that cerebellar abnormalities exist in numerous neurological and psychiatric disorders that degrade not only motor but also cognitive and affective regulation [7–11]. Neuroimaging analyses have confirmed that the cerebellum contributes to all major large-scale functional networks of the brain, including motor networks, attentional (task positive) networks, and default-mode (task negative) network (DMN) [12–16].

Human neuroimaging has provided detailed descriptions of the functional topography of the cerebellar cortex. Stoodley and Schmahmann [17] demonstrated that human cerebellar areas subserving motor functions are distinct from those subserving non-motor and cognitive functions. Motor tasks are largely the domain of the anterior cerebellum, whereas cognitive tasks, such as working memory, are supported by the posterior cerebellum [18]. Several studies using functional MRI have investigated the interactions between human cerebellum and cerebral cortex [19–21]. Task and resting-state fMRI studies have largely supported each other in the functional topography of the cerebellar lobules [12, 21].

Contrasting with the existing detailed knowledge of cerebellar and cerebello-cerebral functional topography, few neuroimaging investigations have focused on characterizing the nature of cerebellar interactions with the cerebral hemispheres, including the possibility that there is a contribution

Qasim Bukhari and Sebastian F. Ruf contributed equally to this work.

✉ Sebastian F. Ruf
s.ruf@northeastern.edu; sebastianfruf@gmail.com

[1] McGovern Institute for Brain Research, Department of Brain and Cognitive Sciences, Massachusetts Institute of Technology, Cambridge, MA, USA

[2] Department of Psychology, Northeastern University, Boston, MA, USA

[3] Department of Electrical and Computer Engineering, Northeastern University, Boston, MA, USA

[4] Department of Neurology, Massachusetts General Hospital and Harvard Medical School, Boston, MA, USA

[5] Alan and Lorraine Bressler Clinical and Research Program for Autism Spectrum Disorder, Massachusetts General Hospital, Boston, MA, USA

[6] Carle Foundation Hospital, Urbana, IL, USA

of cerebellar modulation of brain circuits that is uniform across all domains of behavior (Universal Cerebellar Transform theory, UCT; [22]).

In this work, we estimated effective connectivity using dynamic causal modeling (DCM) in the Human Connectome Project (HCP) dataset to investigate the nature of cerebellar interactions with the cerebral cortex as indexed by resting-state functional connectivity between the cerebellar and cerebral cortex. We evaluated whether within-network DCM relationships (DMN cerebellum—DMN cerebral cortex, task-positive cerebellum—task-positive cerebral cortex, motor cerebellum—motor cerebral cortex) are the same across all networks, as predicted by the Universal Cerebellar Transform (UCT) theory. Additional relationships between and within networks in the cerebellum and the cerebral cortex were also examined.

Materials and Methods

fMRI Data

Data were provided by the Human Connectome Project (HCP), WU-Minn Consortium (Principal Investigators: David Van Essen and Kamil Ugurbil; 1U54MH091657) funded by the 16 NIH Institutes and Centers that support the NIH Blueprint for Neuroscience Research; and by the McDonnell Center for Systems Neuroscience at Washington University [23]. A total of two hundred patients from the HCP were analyzed, with the patients split into two samples of one hundred patients for verification purposes. The first hundred patients were taken from the "100 Unrelated" package provided by the HCP and then a second sex/age-matched group of patients was selected for verification. The hundred unrelated subjects had 54 female and 46 male subjects with 17 aged 22–25, 40 aged 26–30, 42 aged 31–35, and 1 that was 36 +.

The analysis was performed on the first and second preprocessed resting-state scan available for each patient. WU-Minn EPI data was collected using multi-band pulse sequences [24–27]. The default preprocessing pipeline was used [28] which is built upon FSL [29] and FreeSurfer [30]. The prepossessing includes 2 mm spatial smoothing and areal-feature aligned data alignment ("MSMAll") [31]. No additional preprocessing was performed on these data.

ROI Selection

The regions selected for DCM analysis (Fig. 1) were based on functional gradients that are calculated based on diffusion map embedding [32]. These functional gradients were described initially in the cerebral cortex and examined more recently in cerebellar data [13, 14]. Functional gradients
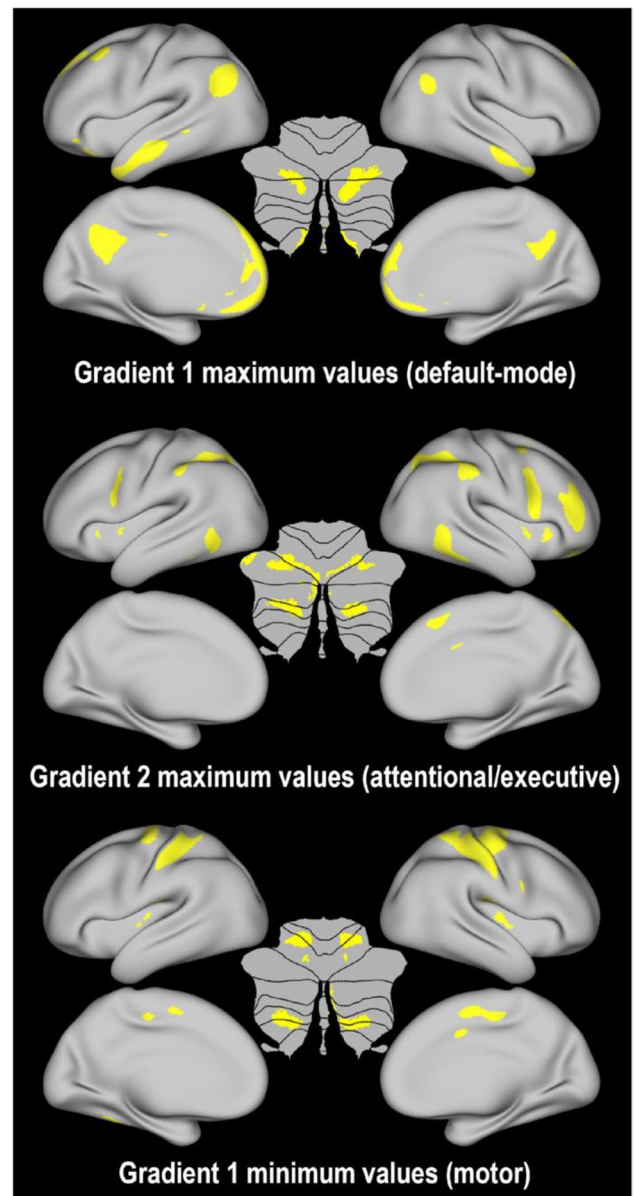

Fig. 1 Cerebellar cortical masks based on functional gradient values calculated from functional connectivity data from cerebellar cortex to cerebral cortex [13, 14] (shown in cerebellar flatamps at the center of each panel), and cerebral cortical masks based on functional connectivity from cerebellar cortex to cerebral cortex (shown in inflated cerebral cortical maps)

were obtained from the freely available datafiles published by Guell and colleagues (https://github.com/xaviergp/cerebellum_gradients). A description of the methodology to generate functional gradients is described in Fig. 2. Top and bottom 5% functional gradient values were chosen as an arbitrary threshold to isolate maximum and minimum values of each functional gradients that isolate specific domains of cerebellar function, as described below. An arbitrary threshold of 5% has also been used elsewhere [13, 14].
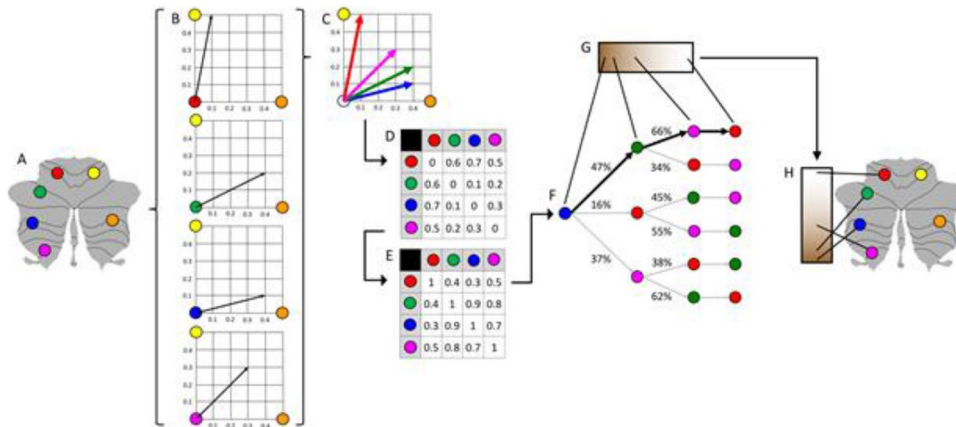
Fig. 2 Schematic representation of calculation of functional gradients using diffusion map embedding. (**A**) This example presents a schematic representation of diffusion map embedding. It illustrates the calculation of the principal functional gradient of 4 cerebellar voxels (red, green, blue, magenta) based on their functional connectivity with two target cerebellar voxels (yellow, orange). (**B**) Connectivity from each cerebellar voxel (red, green, blue, magenta) to the two target cerebellar voxels (yellow, orange) is represented as a two-dimensional vector. (**C**) All vectors can be represented in the same two-dimensional space. (**D**) Cosine distance between each pair of vectors is calculated, and (**E**) an affinity matrix is constructed as (1-cosine distance) for each pair of vectors. This affinity matrix represents the similarity of the connectivity patterns of each pair of voxels. (**F**) A Markov chain is constructed using information from the affinity matrix. Information from the affinity matrix is thus used to represent the probability of transition between each pair of vectors. In this way, there will be higher transition probability between pairs of voxels with similar connectivity patterns. This probability of transition between each pair of vectors can be analyzed as a symmetric transformation matrix, thus allowing the calculation of eigenvectors. (**G**) Eigenvectors derived from this transformation matrix represent the principal orthogonal directions of transition between all pairs of voxels. Here we illustrate the first resulting component of this analysis – the principal functional gradient of our four cerebellar voxels (red, green, blue, magenta) based on their connectivity with our two target cerebellar voxels (yellow, orange) progresses from the blue, to the green, to the magenta, to the red voxel. (**H**) This order is mapped back into our cerebellum map, allowing us to generate functional neuroanatomical descriptions. Of note, our cerebellar functional gradients were calculated using functional connectivity values of each cerebellar voxel with the rest of cerebellar voxels (rather than between four voxels and only two target cerebellar voxels, as in this example). Vectors in our analysis thus possessed many more than just two dimensions, but cosine distance can also be calculated between pairs of high-dimensional vectors. Diffusion map embedding using functional connectivity values from each cerebellar voxel to all cerebellar voxels thus captures the principal gradients of cerebellar functional neuroanatomy. Adapted from [13, 14].

Since here we are interested in evaluating interactions between cerebellum and cerebral cortex, masks in the cerebellum were generated based on functional gradients calculated on functional connectivity data from cerebellar cortex to cerebral cortex (as provided by [13, 14],see second figure in that publication). Cerebellar cortical masks included (i) top 5% values of gradient 1 (which corresponds to default-mode processing); (ii) bottom 5% values of gradient 1 (which corresponds to motor processing); and (iii) top 5% values of gradient 2 (which corresponds to task-focused, attentional/executive processing). These masks are shown in Fig. 1.

Masks in cerebral cortex were obtained by restricting the top 5% values of functional connectivity from the peak voxel of each of the masks in the cerebellar cortex—i.e., voxel with maximum gradient 1 value, voxel with minimum gradient 1 value, and voxel with maximum gradient 2 value. These masks represented areas in cerebral cortex with functional connectivity to cerebellar default-mode, motor, and attentional/executive regions, respectively.

The code used to generate these masks is freely available at http://www.github.com/sfruf/DCM_Cerebellum.

Data Extraction from ROIs

The mean time course of these masks was extracted using HCP workbench (https://www.humanconnectome.org/software/connectome-workbench) and entered into SPM12 (http://www.fil.ion.ucl.ac.uk/spm/software/) to learn a Dynamic Causal Model (DCM) as described in the forthcoming sections.[1] By using the extreme values of functional gradients in the cerebellar cortex that define the poles of functional organization based on connectivity from cerebellum to cerebral cortex (default mode, motor, and attentional processing), and the most strongly connected areas in the cerebral cortex to each of the three areas of interest in the cerebellum, we capture the most important data points for this functional analysis while still considering a sufficiently small network to ensure reasonable DCM results.

---

[1] Note that the traditional implementation of DCM with SPM uses the first eigenvariate instead of the mean. However, in the case of uncentered data, the first eigenvariate points towards the mean so we expect this will not greatly affect our results.

Spectral DCM

In this paper, we use spectral dynamic causal modeling (sDCM)(Friston et al., 2014), a variant of dynamical causal modeling (DCM, [33] which has been proposed specifically for the analysis of resting-state fMRI. sDCM learns a model of the evolution of the neuronal state in n regions, represented by the vector $x \in R^n$, via the observed output from those regions, represented by the vector $y \in R^n$. It is assumed that the model has the following form

$$\dot{x} = Ax + v \tag{1}$$

$$y = h(x, \theta) + e \tag{2}$$

where A captures how neuronal activation spreads between regions, v is neuronal noise, e is measurement noise, and θ is the set of parameters of the hemodynamic response function, $h(x, \theta)$. What differentiates sDCM from other DCM variants that incorporate noise (called stochastic DCM [34]) is that the noise signals v and e are assumed to have spectral density, $g(\omega, \theta)$, which satisfies the following form:

$$g_v(\omega, \theta) = \alpha_v \omega^{-\beta_v} \tag{3}$$

$$g_e(\omega, \theta) = \alpha_e \omega^{-\beta_e} \tag{4}$$

where ω is the frequency, α determines the amplitude of the spectral density, and β captures the decay of the spectral density as frequency increases. For example, for white noise $\beta = 0$ and for pink noise $\beta = 1$.

In order to specify the full generative model, there need to be assumptions on the observation noise, which allows observed cross spectra to be related to the expected cross spectra from the model. Here an additive Gaussian sampling error was used. The full generative model $p(g(\omega), \theta) = p(g(\omega)|\theta)p(\theta|m)$ is then completed by specifying prior beliefs $p(\theta|m)$ about the parameters, which define a particular model m. With the full generative model, one can evaluate the likelihood or the probability of getting some spectral observations given the parameters $p(g(\omega)|\theta)$, as described in depth in Friston et al. (2014).

The full sDCM formulation provides a model of hidden neuronal dynamics which generate complex cross spectra in the measured response. While this could be used to estimate the activity in neuronal populations, the output of the model which will be studied in this paper is the effective connectivity matrix A. As we consider six time courses for inference, this matrix has 36 directed connections between the six ROIs under consideration. These 36 links include connections between regions as well as self-loops which show how an ROI's current activity affects its own future

activity. A positive link from ROI i to ROI j means that activity in ROI i is expected to lead to an increase in activity in ROI j, while a negative link means that activity in ROI i is expected to lead to a decrease in activity in ROI j.

sDCM was motivated by the difficulty in calculating effective connectivity through a typical DCM formulation in resting-state data, which has no external stimuli (Friston et al., 2014). The form of sDCM results in a deterministic formulation which is solved in the frequency domain, which reduces the number of parameters which must be estimated. This has been shown to result in better recovery of true effective connectivity as well as higher sensitivity to changes in the magnitude of edges in the effectivity connectivity matrix on simulated time courses where the underlying effective connectivity is known [35].

The six mean time courses extracted from the HCP workbench were used as input into SPM12 to calculate sDCM, which is implemented in a Bayesian fashion such that all the parameters of the model are given a prior value, which is then updated via data to generate a posterior estimate of the values. The priors on the A matrix were specified as being completely connected. In the next section, we discuss how to move to the connectivity profile at the group level once the individual models had been inverted.

There has been much debate around the complexity of subject-level DCMs (Lohmann et al., 2012). Previous work identified that if there was no prior hypothesis about inter region connectivity, DCM can reasonably infer effective connectivity for less than 8 regions of interest [36]. While this has remained a limitation in the past, recent work using spectral DCM specifically addresses this limitation and successfully identified the effective connectivity between 36 ROIs from a fully connected network (Razi et al., 2017). As such, we expect that the sDCM will be able to infer a reasonable model for each subject using six time courses.

The code used for these analyses is freely available at github.com/sfruf/DCM_Cerebellum.

DCM for Group Analysis

Once the individual level sDCM was computed, SPM routines for Parametric Empirical Bayes (PEB) were used to perform a group-level analysis [37]. Briefly, PEB learns a statistical model of the subject level sDCM parameters θ_1 based on the group level sDCM parameters θ_2 with the following form

$$\theta_1 = \Gamma(\theta_2) + \epsilon_1 \tag{5}$$

$$\theta_2 = \eta + \epsilon_2 \tag{6}$$

where ϵ_1 and ϵ_2 are zero mean Gaussian noise, η is the mean of the group level sDCM parameters, and Γ is a
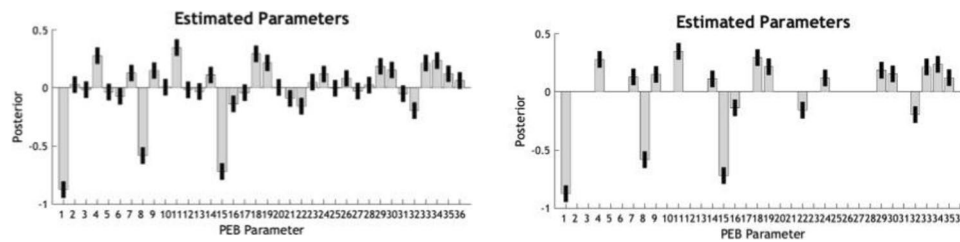
Fig. 3 Posterior Effective Connectivity Estimates. (Left) Effective Connectivity Estimates for all 36 connections between the six regions at the group level. (Right) Effective Connectivity Estimates showing only connections that are non-zero with greater than 0.99 probability

nonlinear function. The output of the PEB analysis is the mean η and noise ϵ_2 which characterize the posterior distribution of the group-level parameters. In practice, the nonlinear function, Γ, which determines how the individual parameters relate to the group level parameters, is taken as a linear model which is characterized by a between-subject design matrix X. Here X was taken to be a matrix with one column of all ones, which ensures that the only group-level parameters returned are the mean sDCM parameters across all two hundred subjects.

The group comparison method used here (PEB) does not specifically rely on the spectral DCM formulation. To the author's best knowledge, it has not been considered in the DCM literature whether there is a relationship between the size of an individual model and the ability to apply PEB. As we have done here, the typical approach is to ensure that each subject level DCM can be reasonably inferred based on model complexity without worrying about the complexity of the comparison. However, given the large number of subjects relative to the model size, we believe that this is a reasonable approach.

Results

The results of the PEB analysis are shown in Figs. 3 and 4. Figure 3 shows the posterior effective connectivity of each of the 36 connections in the group mean sDCM. Figure 4 visualizes the same information as a network, showing the group-level mean interaction pattern thresholded to include only links which have a greater than 0.99 posterior probability, i.e., once the prior on the values have been updated with data there is a probability near 1 that these are non-zero. For greater clarity, the significant links that connect different networks are shown in isolation in Fig. 5.

The effective connectivity matrix shown in Fig. 3 shows that the pattern of within-network coactivation between the cerebellum and the cerebral cortex is shared across all three networks. More specifically, task-positive, motor, and default-mode networks all mutually activate each other in their interaction between cerebellum and cerebral cortex.

We will argue in the "Discussion" section that this finding supports the UCT theory.

Additional relationships were obtained from our analyses. DMN in cerebral cortex and cerebellum as well as task-positive and motor regions in cerebral cortex showed negative self-loops. Negative self-loops match an underlying assumption of the sDCM method, which is that the A matrix corresponds to a stable, continuous time linear system. One way to guarantee that a linear system is stable is for all self-loops to be negative and sufficiently strong; this is due to the fact that for stability to hold in a continuous system, the eigenvalues of A must be strictly negative [38]. There are a number of sufficient conditions for the eigenvalues of A to be strictly negative which can be shown to hold in the presence of strong, negative self-loops (based on matrix analysis tools such as the Gershgorin Disc Theorem among others [39]. In contrast, the motor regions in the cerebellum show a small positive self-loop. This may suggest that there are different intra-cerebellar patterns of motor functional connectivity which can co-activate each other and that are captured in the large-scale mask applied to extract the time course of cerebellar motor functional connectivity. The task-positive regions in the cerebellum have no statistically significant self-loop, however, if the threshold is relaxed sufficiently it can be seen that there is a very small positive self-loop which suggests that a similar organization might be present in the task-positive network.

When looking at between-network relationships between cerebellar cortex and cerebral cortex, networks in the cerebellum tend to co-activate with positive links in both directions between DMN and task-positive as well as task-positive and motor networks. A similar pattern holds in the cerebral cortex, with mutual activation between task-positive and motor networks. Negative links (outside of self-loops) are found when crossing from cerebellum to cerebral cortex or vice versa. Default mode in the cerebellum has a negative interaction both to and from task-positive regions in the cortex suggesting a mutual inhibition of activity. There is a negative link from task-positive network in cerebellum to DMN in cerebral cortex, and a negative link from motor network in cerebral cortex to task-positive network in cerebellum.

Fig. 4 Group mean DCM links with greater than 0.99 probability in the mean of all 200 subjects. Superior panel: Group mean DCM visualized as a network. Red lines correspond to a positive flow of activation, i.e., activation in a given network will lead to an increase in activation in linked networks; blue lines correspond to a negative flow of activation. The link weights correspond to the amount of activation that is spread, so a link with weight 2 results in double the effect of a given amount of activation than a link with weight 1. Thickness of the edges is scaled based on link weight. Notably, within-network interactions between cerebellum and cerebral cortex mutually activate each other in all cases. Inferior panel: Group mean DCM visualized as a matrix. Links that are not significant are shown in white. CC = cerebral cortex. C = cerebellum. Motor = motor network. Task = task-positive network. DMN = default-mode network
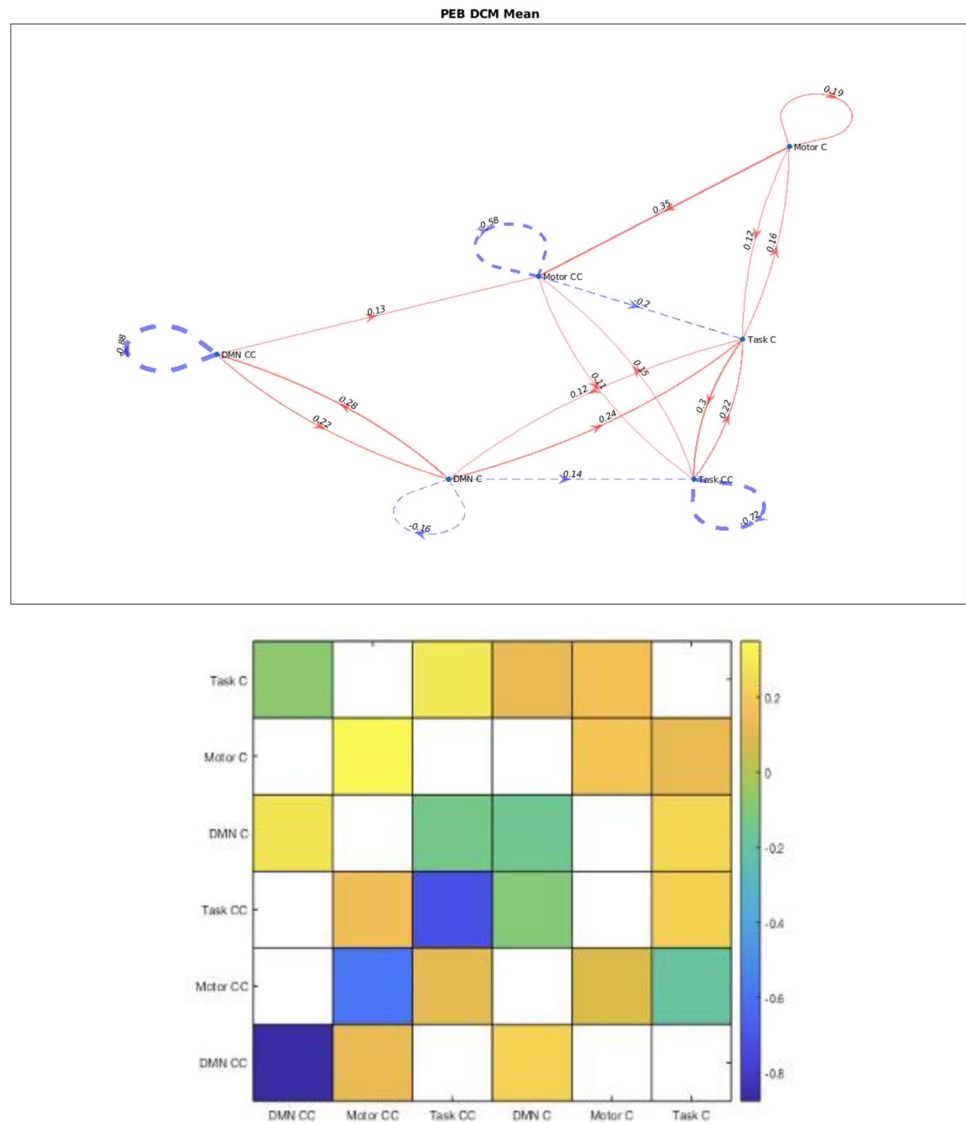

Discussion

Evidence from anatomical, clinical, and neuroimaging studies has established that the cerebellum is implicated in virtually all domains of human behavior, ranging from motor control to cognitive and affective functioning [1]. Functional MRI investigations have delineated distinct territories in the cerebellar cortex [15], as well as other structures in the cerebellum such as the dentate nuclei [40], that are specifically engaged in distinct aspects of movement, thought and emotion regulation. Despite this knowledge, the nature of the contribution of the cerebellum to neurological function has remained difficult to study.

The UCT theory holds that the same neurological process underlies cerebellar modulation of movement, thought, and emotion [2, 3, 13, 14, 41]. This theory is supported by the observations that cerebellar cortex cytoarchitecture is

essentially uniform [42, 43], by clinical observations that there is a similar direction of abnormality in the motor, cognitive, and affective deficits that result from cerebellar injury (Franziska [4–6, 44, 45], and by neuromodulation experiments in humans showing a common pattern of electrophysiological changes in the cerebral cortex after stimulation of different areas of the cerebellar cortex [46]. Alternative views exist in the literature that highlight subtle variations in cerebellar structure [47], or that propose that uniform architecture is not incompatible with distinct computations [48].

The results of the present investigation provide new evidence supporting the UCT theory, and serve as a building ground for future confirmatory analyses. All within-network interactions from cerebellar cortical to cerebral cortical default-mode, task-positive, and motor regions followed the same directionality. Specifically, activation in a given cerebellar network was followed by an increase in activation

Fig. 5 Between-network links in the group mean DCM visualized as a network
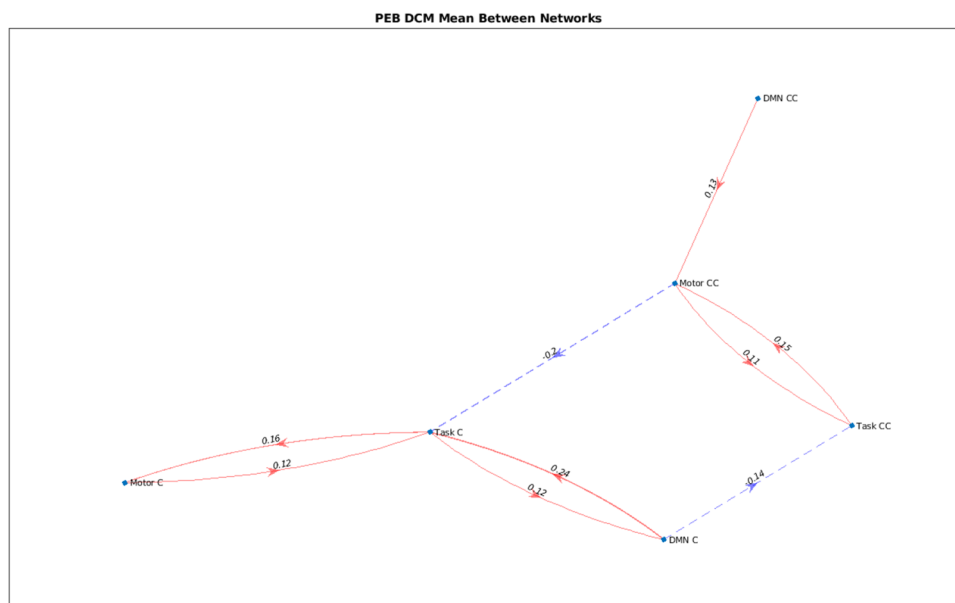
in the linked network in the cerebral cortex as measured by sDCM. A uniform pattern of interaction was not observed from cerebral cortex to cerebellum—specifically, there was not a positive link detected from motor cerebral cortical to motor cerebellar network, while a positive link was detected from default-mode cerebral cortical to default-mode cerebellar network, and a positive link was detected from task-positive cerebral cortical to task-positive cerebellar network. A uniform pattern of interaction from cerebellum to cerebral cortex, but not from cerebral cortex to cerebellum, is the relationship that would be expected based on the theory that a similar neurological process underlies the contribution of the cerebellum to all domains of behavior. Some of the connectivity patterns reported here had also been reported previously; for example, the negative connection between task-positive cerebellum and DMN was also observed in Parker and Razlighi [49].

Our results serve as a building ground for future analyses that are needed in order to validate the findings presented here. While these additional analyses are beyond the scope of this publication, new analytic methods ought to be developed to quantify whether there is a detectable difference in the amount of similarity of within-network interactions from cerebellum to cerebral cortex compared to other network pairs. While our study shows positive links in all cases of cerebellum to cerebral cortical within-network interactions, there was also uniformity in the interactions from cerebral cortex to cerebellum in within-network analyses, with the exception that there was no positive link from cerebral cortical motor network to cerebellar motor network—the absence of such a link is a central result to support our discussion that uniformity in within-network connectivity is unique to the interactions from cerebellum to cerebral cortex. Our results

show for the first time a common nature in the influence that cerebellar networks have in their linked cerebral cortical networks, but more research is needed to definitively establish whether this is a unique feature of the cerebellum, or instead a pattern of positive reinforcement that is equally present in all within-network interactions between all structures in the brain.

Between-network interactions were not uniform in cerebellar cortex (there were bi-directional positive links between motor and task positive, DMN and task positive, but not between motor and DMN cerebellar networks) or between cerebellar cortex and cerebral cortex (there was a negative link from cerebral cortical motor to cerebellar task network, and a negative link from cerebellar default-mode to cerebral cortical task-positive network, but no other between-network significant links detected between cerebellum and cerebral cortex). Our interpretation is that non-uniform interactions between different network kinds (e.g., between default-mode and task-positive networks) are not against the notion of a UCT, but are instead consistent with the well-established knowledge that interactions between different network kinds are not uniform in the brain. For example, it is well established that there is a negative relationship between default-mode and task-positive networks in the brain [50]—this relationship was detected in our study between cerebellar default-mode and cerebral cortical task-positive network—and that such a relationship is not equally present between other network kinds. In this way, finding different kinds of interactions between networks of different kinds is not an argument against the notion of a UCT, and instead provides an example of how a modular organization of the cerebellum—where distinct networks with different patterns of between-network interactions exist within the

cerebellum—is compatible with the notion of a UCT where there is a similar neurological process underlying cerebellar modulation of extra-cerebellar activity, as indexed by our analyses of within-network connectivity from cerebellum to cerebral cortex. The same logic applies to the differences observed in self-loop interactions between cerebellar motor network and cerebellar default-mode and task-positive self-loop interactions.

Declarations

Conflict of Interest The authors declare no competing interests.

References

1. Schmahmann J, Guell X, Stoodley C, Halko M. The theory and neuroscience of cerebellar cognition. Annu Rev Neurosci. 2019;42:337–64.

2. Schmahmann JD. The cerebrocerebellar system: anatomic substrates of the cerebellar contribution to cognition and emotion. Int Rev Psychiatry. 2001;13(4):247–60. https://doi.org/10.1080/09540260120082092.

3. Guell X, Hoche F, Schmahmann JD. Metalinguistic deficits in patients with cerebellar dysfunction: empirical support for the dysmetria of thought theory. Cerebellum. 2015;14(1):50–8. https://doi.org/10.1007/s12311-014-0630-z.

4. Hoche F, Guell X, Sherman JC, Vangel MG, & Schmahmann JD. Cerebellar contribution to social cognition. Cerebellum. 2016;15(6). https://doi.org/10.1007/s12311-015-0746-9.

5. Hoche F, Guell X, Sherman JC, Vangel MG, Schmahmann JD. Cerebellar contribution to social cognition. Cerebellum. 2016;15(6):732–43. https://doi.org/10.1007/s12311-015-0746-9.

6. Schmahmann JD, Sherman JC. The cerebellar cognitive affective syndrome. Brain. 1998;141(May 1998):561–79. https://doi.org/10.1093/brain/121.4.561.

7. Anteraper SA, Guell X, D'Mello A, Joshi N, Whitfield-Gabrieli S, Joshi G. Disrupted cerebrocerebellar intrinsic functional connectivity in young adults with high-functioning autism spectrum disorder: a data-driven, whole-brain, high-temporal resolution functional magnetic resonance imaging study. Brain Connectivity. 2019;9(1):48–59. https://doi.org/10.1089/brain.2018.0581.

8. Dong D, Luo C, Guell X, Wang Y, He H, Duan M, Eickhoff SB, & Yao D. Compression of cerebellar functional gradients in schizophrenia. Schizophrenia Bull. 2020.https://doi.org/10.1093/schbul/sbaa016.

9. Guo CC, Tan R, Hodges JR, Hu X, Sami S, Hornberger M. Network-selective vulnerability of the human cerebellum to Alzheimer's disease and frontotemporal dementia. Brain. 2016;139(5):1527–38. https://doi.org/10.1093/brain/aww003.

10. Jacobs HIL, Hopkins DA, Mayrhofer HC, Bruner E, Van Leeuwen FW, Raaijmakers W, Schmahmann JD. The cerebellum in Alzheimer's disease: evaluating its role in cognitive decline. Brain. 2018;141(1):37–47. https://doi.org/10.1093/brain/awx194.

11. Stoodley CJ, D'Mello AM, Ellegood J, Jakkamsetti V, Liu P, Nebel MB, Gibson JM, Kelly E, Meng F, Cano CA, Pascual JM, Mostofsky SH, Lerch JP, & Tsai PT. Altered cerebellar connectivity in autism and cerebellar-mediated rescue of autism-related behaviors in mice. Nat Neurosci. 2017. https://doi.org/10.1038/s41593-017-0004-1.

12. Buckner R, Krienen F, Castellanos A, Diaz JC, Yeo BT. The organization of the human cerebellum estimated by intrinsic functional connectivity. J Neurophysiol. 2011;106:2322–45. https://doi.org/10.1152/jn.00339.2011.

13. Guell X, Gabrieli JDE, Schmahmann JD. Embodied cognition and the cerebellum: perspectives from the dysmetria of thought and the universal cerebellar transform theories. Cortex. 2018;100:140–8. https://doi.org/10.1016/j.cortex.2017.07.005.

14. Guell X, Schmahmann J, Gabrieli J, Ghosh S. Functional gradients of the cerebellum. Elife. 2018;7:e36652. https://doi.org/10.7554/eLife.36652.

15. Guell X, Schmahmann J. Cerebellar functional anatomy: a didactic summary based on human fMRI evidence. Cerebellum. 2019. https://doi.org/10.1007/s12311-019-01083-9.

16. King M, Hernandez-Castillo CR, Poldrack RA, Ivry RB, Diedrichsen J. Functional boundaries in the human cerebellum revealed by a multi-domain task battery. Nat Neurosci. 2019;22:1371–8. https://doi.org/10.1038/s41593-019-0436-x.

17. Stoodley CJ, Schmahmann JD. Functional topography in the human cerebellum: a meta-analysis of neuroimaging studies. Neuroimage. 2009;44(2):489–501. https://doi.org/10.1016/j.neuroimage.2008.08.039.

18. Stoodley CJ, Valera EM, Schmahmann JD. Functional topography of the cerebellum for motor and cognitive tasks: an fMRI study. Neuroimage. 2012;59(2):1560–70. https://doi.org/10.1016/j.neuroimage.2011.08.065.

19. Habas C, Kamdar N, Nguyen D, Prater K, Beckmann CF, Menon V, Greicius MD. Distinct cerebellar contributions to intrinsic connectivity networks. J Neurosci. 2009;29(26):8586–94. https://doi.org/10.1523/JNEUROSCI.1868-09.2009.

20. Krienen FM, Buckner RL. Segregated fronto-cerebellar circuits revealed by intrinsic functional connectivity. Cerebral Cortex (New York, NY: 1991). 2009;19(10):2485–97. https://doi.org/10.1093/cercor/bhp135.

21. O'Reilly JX, Beckmann CF, Tomassini V, Ramnani N, Johansen-Berg H. Distinct and overlapping functional zones in the cerebellum defined by resting state functional connectivity. Cerebral Cortex (New York, NY: 1991). 2010;20(4):953–65. https://doi.org/10.1093/cercor/bhp157.

22. Schmahmann JD. From movement to thought: anatomic substrates of the cerebellar contribution to cognitive processing. Hum Brain Mapp. 1996;4(3):174–98. https://doi.org/10.1002/(SICI)1097-0193(1996)4:3%3c174::AID-HBM3%3e3.0.CO;2-0.

23. Van Essen DC, Smith SM, Barch DM, Behrens TEJ, Yacoub E, Ugurbil K. The WU-Minn human connectome project: an overview. Neuroimage. 2013;80:62–79. https://doi.org/10.1016/j.neuroimage.2013.05.041.

24. Feinberg DA, Moeller S, Smith SM, Auerbach E, Ramanna S, Gunther M, Glasser MF, Miller KL, Ugurbil K, Yacoub E. Multiplexed echo planar imaging for sub-second whole brain FMRI and fast diffusion imaging. PLoS ONE. 2010;5(12):e15710. https://doi.org/10.1371/journal.pone.0015710.

25. Moeller S, Yacoub E, Olman CA, Auerbach E, Strupp J, Harel N, Uğurbil K. Multiband multislice GE-EPI at 7 tesla, with 16-fold acceleration using partial parallel imaging with application to high spatial and temporal whole-brain fMRI. Magn Reson Med. 2010;63(5):1144–53. https://doi.org/10.1002/mrm.22361.

26. Setsompop K, Gagoski BA, Polimeni JR, Witzel T, Wedeen VJ, Wald LL. Blipped-controlled aliasing in parallel imaging for simultaneous multislice echo planar imaging with reduced g-factor penalty. Magn Reson Med. 2012;67(5):1210–24. https://doi.org/10.1002/mrm.23097.

27. Xu J, Moeller S, Auerbach EJ, Strupp J, Smith SM, Feinberg DA, Yacoub E, Uğurbil K. Evaluation of slice accelerations using multiband echo planar imaging at 3 T. Neuroimage. 2013;83:991–1001. https://doi.org/10.1016/j.neuroimage.2013.07.055.

28. Glasser MF, Sotiropoulos SN, Wilson JA, Coalson TS, Fischl B, Andersson JL, Xu J, Jbabdi S, Webster M, Polimeni JR, Van Essen DC, Jenkinson M, WU-Minn HCP Consortium. The minimal pre-processing pipelines for the Human Connectome Project. Neuroimage. 2013;80:105–24. https://doi.org/10.1016/j.neuroimage.2013.04.127.

29. Jenkinson M, Beckmann CF, Behrens TEJ, Woolrich MW, Smith SM. FSL. Neuroimage. 2012;62(2):782–90. https://doi.org/10.1016/j.neuroimage.2011.09.015.

30. Fischl B. FreeSurfer. Neuroimage. 2012;62(2):774–81. https://doi.org/10.1016/j.neuroimage.2012.01.021.

31. Robinson EC, Jbabdi S, Glasser MF, Andersson J, Burgess GC, Harms MP, Smith SM, Van Essen DC, Jenkinson M. MSM: a new flexible framework for Multimodal Surface Matching. Neuroimage. 2014;100:414–26. https://doi.org/10.1016/j.neuroimage.2014.05.069.

32. Coifman RR, Lafon S, Lee AB, Maggioni M, Nadler B, Warner F, Zucker SW. Geometric diffusions as a tool for harmonic analysis and structure definition of data: multiscale methods. Proc Natl Acad Sci. 2005;102(21):7432–7. https://doi.org/10.1073/pnas.0500896102.

33. Friston KJ, Harrison L, Penny W. Dynamic causal modelling. Neuroimage. 2003;19(4):1273–302. https://doi.org/10.1016/s1053-8119(03)00202-7.

34. Daunizeau J, Stephan KE, & Friston KJ. Stochastic dynamic causal modelling of fMRI data: should we care about neural noise? NeuroImage. 2012.https://doi.org/10.1016/j.neuroimage.2012.04.061.

35. Razi A, Kahan J, Rees G, Friston KJ. Construct validation of a DCM for resting state fMRI. Neuroimage. 2015;106:1–14. https://doi.org/10.1016/j.neuroimage.2014.11.027.

36. Seghier ML, Friston KJ. Network discovery with large DCMs. Neuroimage. 2013;68:181–91. https://doi.org/10.1016/j.neuroimage.2012.12.005.

37. Friston KJ, Litvak V, Oswal A, Razi A, Stephan KE, van Wijk BCM, Ziegler G, Zeidman P. Bayesian model reduction and empirical Bayes for group (DCM) studies. Neuroimage. 2016;128:413–31. https://doi.org/10.1016/j.neuroimage.2015.11.015.

38. Hespanha JP. Linear systems theory. Princeton University Press; 2009.

39. Horn RA. Matrix analysis (2nd edition). Cambridge University Press; 2012.

40. Guell X, D'Mello AM, Hubbard NA, Romeo RR, Gabrieli JDE, Whitfield-Gabrieli S, Schmahmann JD, Anteraper SA. Functional territories of human dentate nucleus. Cereb Cortex. 2019. https://doi.org/10.1093/cercor/bhz247.

41. Schmahmann J. An emerging concept: the cerebellar contribution to higher function. Arch Neurol. 1991;48(11):1178–87. https://doi.org/10.1001/archneur.1991.00530230086029.

42. Ito M. Movement and thought: identical control mechanisms by the cerebellum. Trends Neurosci. 1993;16(11):448–50. https://doi.org/10.1016/0166-2236(93)90073-U.

43. Voogd J, Glickstein M. The anatomy of the cerebellum. Trends Cogn Sci. 1998;2(9):307–13. https://doi.org/10.1016/S1364-6613(98)01210-8.

44. Hoche F, Guell X, Vangel M, Sherman J, Schmahmann J. The cerebellar cognitive affective/Schmahmann syndrome scale. Brain. 2018;141(1):248–70.

45. Schmahmann JD, Weilburg JB, Sherman JC. The neuropsychiatry of the cerebellum—insights from the clinic. Cerebellum. 2007;6(3):254–67. https://doi.org/10.1080/14734220701490995.

46. Farzan F, Pascual-Leone A, Schmahmann JD, & Halko M. Enhancing the temporal complexity of distributed brain networks with patterned cerebellar stimulation. Sci Rep. 2016;6. https://doi.org/10.1038/srep23599.

47. Cerminara NL, Lang EJ, Sillitoe RV, Apps R. Redefining the cerebellar cortex as an assembly of non-uniform Purkinje cell microcircuits. Nat Rev Neurosci. 2015;16(2):79–93. https://doi.org/10.1038/nrn3886.

48. Diedrichsen J, King M, Hernandez-Castillo C, Sereno M, Ivry RB. Universal transform or multiple functionality? Understanding the contribution of the human cerebellum across task domains. Neuron. 2019;102(5):918–28. https://doi.org/10.1016/j.neuron.2019.04.021.

49. Parker DB, Razlighi QR. Task-evoked negative BOLD response and functional connectivity in the default mode network are representative of two overlapping but separate neurophysiological processes. Sci Rep. 2019;9(1):14473. https://doi.org/10.1038/s41598-019-50483-8.

50. Fox MD, Snyder AZ, Vincent JL, Corbetta M, Van Essen DC, Raichle ME. The human brain is intrinsically organized into dynamic, anticorrelated functional networks. Proc Natl Acad Sci. 2005;102(27):9673–8. https://doi.org/10.1073/pnas.0504136102.